Planetary Entry Body Heating Rate Measurements in Air and Venus Atmospheric Gas up to T = 15,000°K

F. R. Livingston* and J. W. Williard†
Jet Propulsion Laboratory, Pasadena, Calif.

Convective plus radiative shock-tube-model stagnation-point heating rate measurements are presented. Platinum thick-film calorimeter gages, both uncoated and carbon-coated, sensed the heat flux on the external surface of the hemispherical and truncated-cylinder models. This thorough experimental study of total heat flux provides quantitative data necessary to verify existing theoretical radiative flowfield methods. In contrast with past experiments, the radiative flux emanating from a 2π sterad solid angle at all wavelengths is a significant fraction of the total heating measured by the calorimeter. Experimental thermochemical and geometric conditions are systematically changed in order to interpret the results in terms of convective heating, radiative heating, and coupling effects. At temperatures between 12,000 and 15,000°K, the measurements agree with theoretical uncoupled convective heating summed with isothermal radiative flux reduced by a radiative cooling factor. At lower temperatures, the measured heating was more than expected, especially in air.

Nomenclature

a = speed of sound in gas
C = specific heat of gage material
E = voltage drop across the gage element
F = radiative flux
H = enthalpy
I = current through calorimeter gage
= radiative intensity
P = pressure
Q = heat-transfer rate
R_0 = resistance of gage element at 0°C
R = nose radius of model
r^* = truncated cylinder radius
U_R = reflected shock velocity
U_s = shock velocity
l = thickness of gage
t = time
x = coordinate along body surface
y = coordinate normal to body surface
α_0 = temperature coefficient of electrical resistance at 0°C
δ = bow shock standoff distance
ρ = density
$( )_1$ = property evaluated at the initial thermodynamic state of the gas in the shock tube
$( )_2$ = property evaluated at the thermodynamic state behind the incident shock in the shock tube
$( )_3$ = property evaluated at the thermodynamic state behind a standing model bow shock
$( )_s$ = property of gas at the stagnation point of flow
$( )_w$ = property at wall temperature of the model and stagnation pressure
$( )_5$ = property evaluated behind a reflected shock wave

I. Introduction

THERE has been at least a factor-of-2 uncertainty in the amount of radiative emission, from the bow shock layer, which would reach an entry vehicle surface on a braking maneuver in the atmosphere of Venus or Earth especially at speeds faster than 30,000 fps. It is a very difficult problem to estimate the heat flux at the surface of a planetary entry probe when a strong radiation field exists within the fluid flowfield surrounding the body; however, several investigators have solved special cases of this problem. Excellent reviews of the effort expended in understanding the problem have been recently made by Goulard et al.[1] and Anderson.[2] The theoretical difficulty in solving the radiation coupled flowfield problem lies in its complexity—the simultaneous solution of the fluid mechanical conservation equations with the equation of radiative transport. The amount of far-ultraviolet flux reaching a body surface is the most uncertain heat-transfer quantity because of the strong absorption in these bands and their extreme sensitivity to shock-layer temperature. The sparsity of radiative intensity or flux measurements at far-ultraviolet wavelengths where self-absorption has an important effect in a nonadiabatic flowfield is one reason for the present uncertainty. This paper attempts to add new experimental information with which to verify existing theories.

The present experiment has been designed to model the stagnation region of a planetary entry body and to subject this region to the hot shock-layer flow that would exist in flight. A shock tube momentarily generates the heated gas and drives this gas over the truncated (flat-faced) cylindrical or hemispherical model while a stagnation-point-mounted calorimeter gage is being monitored. In this experiment, the heat flux sensing surface—a thick-film platinum calorimeter, either uncoated or carbon-coated—is directly adjacent to the radiative field and also the flowfield of the shock-heated test gas. The model stagnation-point heating measurements in a 90% CO_2–10% N_2 mixture and in air were obtained at incident shock velocities of from 18,000 to 30,000 fps in a shock tube, which correspond to flight speeds of from 25,000 to 41,000 fps.

II. Experiment

Shock Tubes

The tests were conducted in two 6-in.-diam shock tubes utilizing a 12-in.-diam free-piston driver[3] and a 1.4-in.-diam arc discharge driver.[4] The vast majority of the measurements were obtained in a free jet flowing out of the 6-in.-diam free-piston driven tube. The experimental setup as used for

Presented as Paper 69-635 at the AIAA 4th Thermophysics Conference, San Francisco, Calif., June 16–18, 1969; submitted February 16, 1970; revision received August 20, 1970. This paper presents the results of one phase of research carried out at the Jet Propulsion Laboratory, Caltech, under Contract NAS 7-100, sponsored by NASA.

* Supervisor, Aerothermodynamics Group, Aerophysics Section. Member AIAA.

† Research Engineer; now at the Plasma Physics Laboratory, Princeton University.

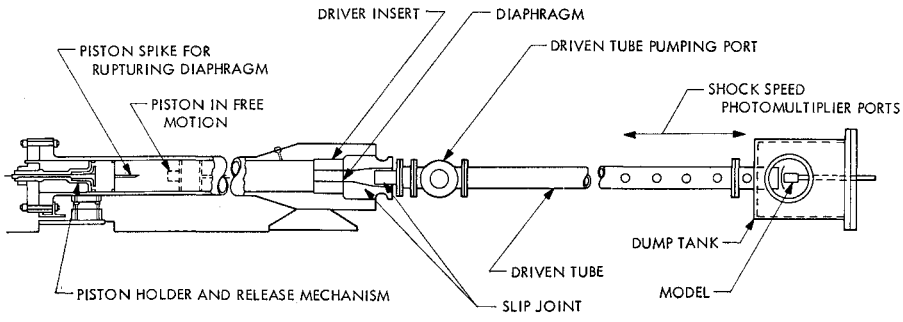

Fig. 1 Schematic of experimental apparatus.

most of the runs is shown in Fig. 1. The free-piston driver has a 12-in.-diam piston that is used to compress the driver gas to final pressures up to 7600 psia. By using helium and helium-nitrogen driver gas mixtures it was possible to cover the 18,000 to 30,000 fps shock speed range required for the experiment. The driven tube consisted of 32 ft of 6-in.-diam stainless-steel tubing with regularly spaced instrument ports for measuring shock speed. The driven tube is terminated in a 24-in.-diam dump tank. Models were sting- or sector-mounted in the dump tank at distances of $\frac{3}{8}$ to $\frac{3}{4}$ in. from the exit orifice of the shock tube.

Models

Calorimeter heat-transfer models of the type developed by Rose[5] were used in the experiment. The models used were $1\frac{1}{4}$-, 2-, and $2\frac{1}{2}$-in.-diam truncated cylinders and 5-in.-diam hemispheres (Fig. 2).

In the present work, much use is made of truncated-cylinder models rather than hemisphere models in order to maximize the ratio of radiative flux to convective heat flux for a given model diameter. The larger ratio of radiative flux to convective flux occurs because the flat-faced body has a shock standoff distance over four times that of a hemisphere of the same diameter (leading to a proportional increase in optical depth of the shock layer). The stagnation-point velocity gradient is about 0.2 that of a hemisphere with comparable diameter, resulting in a convective heating only $0.2^{1/2}$ that of the hemisphere. One disadvantage in using the truncated-cylinder model is that the flowfield about the shape is not as well-known as that about a hemisphere.

In constructing the truncated-cylinder models, platinum strips were pulled through slots centered in $\frac{1}{8}$-in.-thick by $1\frac{1}{4}$-in.-diam glass disks. The strips were taped flush on the front surface and 28 gage wire leads soldered onto the tabs protruding through the slots. Tension was then maintained on these wires while the back of the gage was sealed with a dome of epoxy. After curing, the tape on the front face was carefully removed with acetone and the slots filled with epoxy. During use these units were cemented to the face of the model holder. By use of the collars shown in Figs. 2b and 2d, the same type of Pyrex disk could be used for the three cylindrical models. After use the Pyrex disk was broken from the holder and a new unit installed. Depending on the initial tightness of the gage and the size of the model being used, gage life was from 1 to 3 runs.

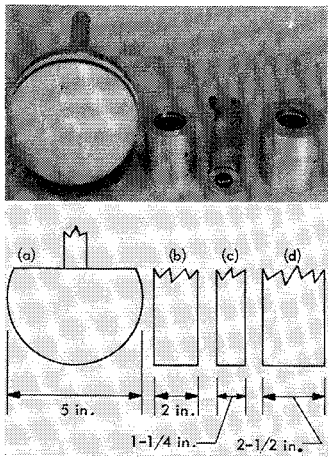

Fig. 2 Calorimeter heat-transfer models: a) hemispherical model, b) 2-in.-diam collar, c) $1\frac{1}{4}$-in.-diam truncated-cylinder model, d) $2\frac{1}{2}$-in.-diam collar.

The hemisphere models (Fig. 2a) were usually constructed with 1 gage. One model used had 17 gages placed in rows at angles up to 45° from the model centerline. During use each gage was moved to the stagnation point by rotating and pitching the model. Gages not in use were covered to prevent damage until use. As with the truncated-cylinder models, the slots adjacent to the gage were filled with epoxy. The insides of the hemisphere were filled with RTV 20 silicone rubber to increase the strength.

The calorimeter gages used were sufficiently thin, l = 0.0005-in., that the temperature increase of the gage was proportional to the heat flux transferred to it. Thus by maintaining a constant current I, usually 1.50 amp, the voltage rate of change, dE/dt, was related to the heat-transfer rate by $Q = (C\rho l/\alpha_0 R_0 I)\ (dE/dt)$. In order to minimize the influence of gage uncertainties on the final data, the length, width, and weight of each platinum strip was carefully measured and recorded. Using these measurements, the density-thickness product (ρl) was determined from known quantities. Prior to each run, the voltage drop across the exposed area of the gage was carefully measured using a microvoltmeter and two small probes. The test value of gage current was used during this measurement; thus the resistance value R_0 of the exposed gage element could be accurately computed. The value of the temperature coefficient of electrical resistivity (3.92×10^{-3}/C°), previously determined by Horton and Babineaux[6] at this laboratory, was used in all computations. The value of the specific heat C was taken as 9.032 cal/C°/g as reported for commercially pure platinum. In order to assure that Joule heating was not a factor in gage response, a model was tested in a bell jar over a wide range of conditions. Air pressure was varied from 0.001 to 760 mm Hg and current from 0.1 to 4.8 amp. Gage response for a minimum of 5 min at each condition was recorded. The results indicated a negligible influence at the experimental test conditions (pressure = 0.25 mm Hg, current = 1.5 amp). Since the platinum metal is highly reflective at the near-infrared wavelengths and absorbs most of the incident radiation in the far-ultraviolet, a carbon coating was sputtered on some gages to get a more flat response with wavelength. Absorptance of carbon films on platinum obtained at this, laboratory[7] is about 80% at wavelengths from 0.2 to 0.7μ and is identical to massive graphite. The results for two- and three-layer films were identical from 0.2 to 2.7μ wavelength, whereas beyond 0.7μ, the single-layer films exhibited considerable more variation. A single carbon film is less than 1μ thick.

In a typical run, a model is attached to the sting and fastened in the dump tank at the downstream end of the free-piston shock tube. An image-converter camera photograph of the model is then taken for position reference as shown in

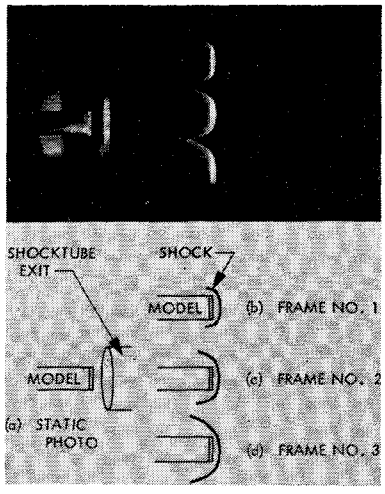

Fig. 3 Image converter camera photograph of truncated 1¼-in.-diam truncated-cylinder model: a) static calibration, b) flow at U_s = 20,400 fps 8 μsec after start, c) 13 μsec after start, d) 23 μsec after start.

Fig. 3a. Upon closing the dump tank and shock tube, the system is pumped to a pressure of 10^{-5} mm Hg and held until filling with 0.25 mm Hg of air or Venus atmosphere gas.

The current is applied to each gage for several minutes before firing to allow stabilization of the circuit. Gage current is then checked after insertion of the test gas and immediately prior to firing.

When all recording oscilloscopes are ready, the operator releases the driver piston, thus compressing the driver gas and rupturing the steel or brass diaphragm. The driver gas accelerates through the broken diaphragm into the driven tube, forcing the air or Venus gas to move toward the model at high velocity. An incident shock wave precedes the moving gas. The test gas relaxation process is sensed by sidewall photomultiplier tubes monitoring visible radiation emission normal to the flow direction. Oscillographs, shown in Fig. 4, illustrate the flow regions passing the optical slit entrance to the phototube. First the radiation overshoot is seen, followed by test gas that has reached thermochemical equilibrium, and finally the cool driver gas comes into view. These collimated photomultiplier tubes spaced at regular intervals were also used to measure the shock speed. Oscilloscope time base generators were calibrated daily to assure accurate measurement of shock speeds within ±0.5%. When using the free-piston driver, final driver gas conditions are a known constant value. Therefore, test conditions were easily predicted and run-to-run shock speed variation was less than 2.0%.

A good portion of the shock-heated test gas is decelerated by a viscous wall-boundary layer and is effectively removed from the hot test slug. Many otherwise good runs are ruined when the test slug is of insufficient length for the model flowfield to approach a steady-state condition. When the hot test gas emerges from the end of the shock tube, it encounters the model, as shown in Fig. 3b, taken 8 μsec after shock impingement. In this particular run the incident shock has a velocity of 20,400 fps in air. The incident shock wave partially reflects and the remainder propagates past the model unimpeded as the shock layer forms about the model, shown in Fig. 3c, 13 μsec after shock impingement. The reflected bow shock, separating the body shock layer from the oncoming test gas encounters the driver gas interface 23 μsec after shock reflection, as seen in Fig. 3d. Simultaneous with shock reflection, we assume shock-layer flow starts about the model, progresses, and nears the equilibrium thermochemical conditions; however, there is still doubt as to the time necessary to establish flow within the shock layer. It is during the time after the model flowfield reaches its near-equilibrium conditions and before the driver gas approaches that the heat-transfer measurement is made. A voltage change proportional to the temperature of the platinum calorimeter is recorded on an oscillograph, using a differentially balanced preamplifier gage circuit. An example is shown in Fig. 5.

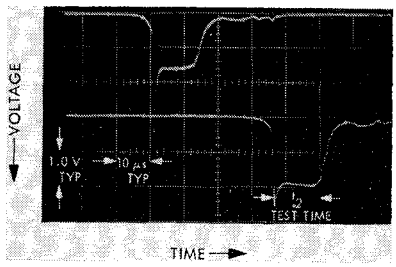

Fig. 4 Oscillograph of two sidewall phototube outputs: U_s = 28,600 fps in 90% CO_2-10% N_2.

III. Model Flowfield Analysis

Flowfield Thermochemistry

The equilibrium thermochemical state of the shock tube and shock-layer plasma was computed by the method of Horton and Menard[8] and published in Refs. 9 and 10. We here assume that the state of the gas throughout the test slug, the bow shock layer, and the reflected shock region was uniform. The computer program also supplied equilibrium chemical composition for these conditions. The predominant chemical species are nitrogen and oxygen atoms for air and oxygen, carbon, and nitrogen atoms for Venus atmosphere. Because of the two-shock compression of the shock layer gases in the shock tube, the simulated flight velocity is a factor of 1.37 greater than the shock velocity (for equal stagnation enthalpy).

Bow Shock Formation

Because of the necessity of knowing when the flowfield about the model has neared a stabilized condition, the radiating shock layer is photographed on most runs. The reflected shock from all models takes the form of a spherical segment after reaching a near-stable position, but there is a marked difference in the form and speed of the reflected shock for the two model shapes. The reflected shock off the hemispherical model starts and remains a near-spherical segment as it approaches the equilibrium position. Figure 12 illustrates the dependence of the position of the reflected bow shock with time for the hemispherical model. The ordinate is the distance y of the shock from the stagnation point, normalized by the equilibrium shock standoff distance computed by the method of Serbin[11] $\delta = 2R/3(\rho_3/\rho_2 - 1)$. The abscissa of Fig. 6 is the time t measured from the incident shock impingement, normalized by the theoretical time required for the unattenuated reflected normal shock wave in an equilibrium gas to propagate from the stagnation point to the Serbin standoff distance, $\tau = \delta/U_R$. The data from the runs shown

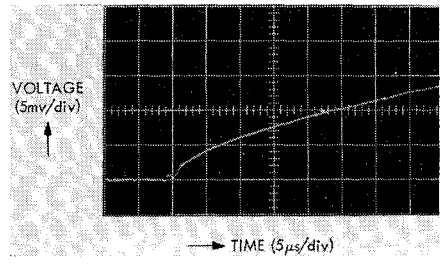

Fig. 5 Oscillograph of 1¼-in.-diam truncated-cylinder heat transfer record at U_s = 22,000 fps.

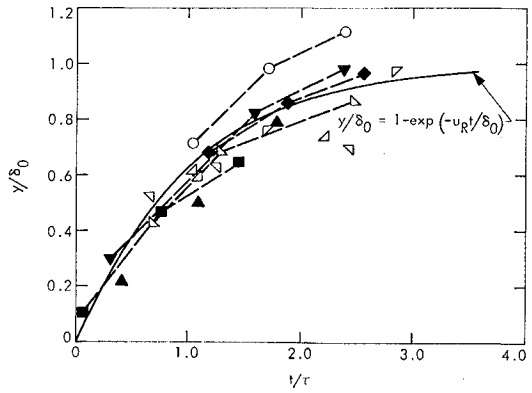

Fig. 6 Reflected bow shock on 5-in.-diam hemisphere; filled symbols indicate air data.

in Fig. 6 in both air and 90% CO_2–10% N_2 are closely approximated by a curve allowing for an exponential decay of the bow shock velocity with a time constant τ.

The bow shock reflects off the flat-faced models much differently. The bow shock moves away from the body at nearly constant velocity for the time required for the head of an expansion wave to propagate at sonic velocity a_5 from the outer edge to the stagnation point. A study of the shock position y/δ data plotted as a function of the time t/τ for the flat-faced cylinder model shown in Fig. 7 leads to the preceding observation. Fortuitously for these test conditions, the time required for the expansion wave to propagate from the model edge to the stagnation-point streamline is almost equal to the incremental time necessary for the bow shock to reach an equilibrium position. Therefore, the bow shock is formed very rapidly. The shock standoff distance δ was found to be approximately that computed by Serbin for the test times of these runs; i.e., $\delta = 1.03 r^*/(\rho_3/\rho_2 - 1)^{1/2}$.

From the foregoing evidence we believe we have found the criteria to determine when the bow shock has approached the equilibrium position, and hence can interpret the heating rate measurements correctly. The flow starting times indicated on the heat-transfer traces agree with those found optically.

Uncoupled Convective Heat Transfer

Certain investigators concerned with the planetary entry problem have attempted to calculate and measure the uncoupled convective heat-transfer rates at the stagnation point of blunt bodies. Experimental heating rates have been measured at the stagnation point of small hemispherical models in shock tubes, where radiative flux was minimized, and were

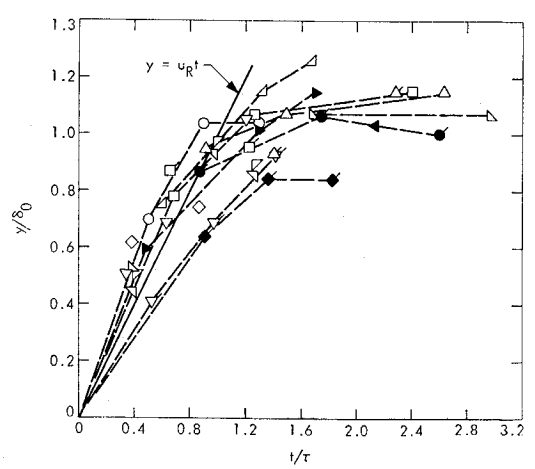

Fig. 7 Reflected bow shock on truncated-cylinder models; filled symbols indicate air data.

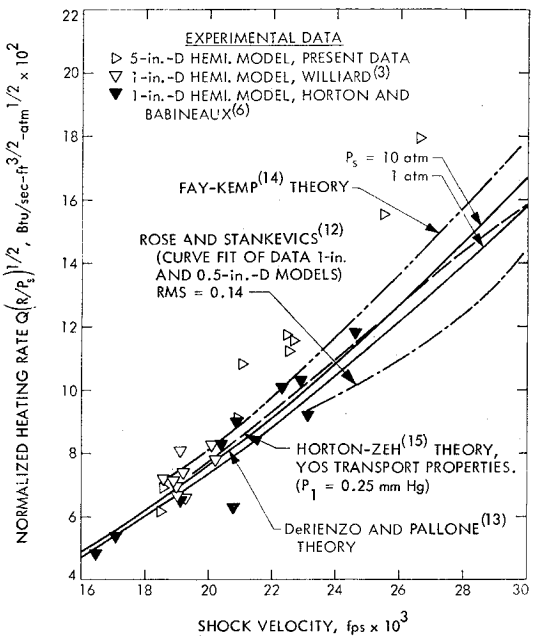

Fig. 8 Stagnation-point heating rates of shock-tube models in air; $P_1 = 0.25$ torr where not indicated otherwise.

found to be in agreement with theoretical calculations. In making these measurements, the magnitude of convective heating rates to the models in air has been established within a probable error of 10% at least to shock speeds of 25,000 fps. Some previous shock-tube-model heat-transfer results in air, shown in Fig. 8, illustrate the agreement between experiment and the theory for 1-in.-diam hemispherical models. All the data points shown were obtained at this laboratory[3,6] at an initial pressure of 0.25 mm Hg. The present data obtained on a 5-in.-diam hemispherical model are generally greater than the remainder of the data and a portion of this excess is attributed to radiative flux. As seen in this figure, the shock-tube results of Rose and Stankevics[12] fall somewhat below the theory of DeRienzo and Pallone[13] at shock speeds near 28,000 fps, however, the scatter of the data was 15%—equivalent to the largest discrepancy. Other theoretical calculations are within 10% of DeRienzo and Pallone, including the theoretical results of Fay-Kemp[14] and Horton and Zeh[15] of this laboratory, which are seen in the figure to be in very close agreement. Thus, it follows that convective heat-transfer rates to hemispherical bodies in air are well estimated by the theory of DeRienzo and Pallone at these test conditions and hence will be used to analyze the present results.

For the Venus atmospheric gas, the theoretical methods of Van Tassell[16] and Hoshizaki[17] were compared with the available heat-transfer data from shock-tube tests with small hemispherical models, as seen in Fig. 9. Two data points obtained by Gruszczynski and Warren[18] are shown and do not favor either theory. The 100% CO_2 data obtained principally by Nerem[19] and Collins-Horton[20] scatter ±10% about some mean which would lie in the region enclosed by the two theories, favoring the theory of Hoshizaki at these lower shock speeds and that of Van Tassell at the higher shock velocity. Van Tassell indicated very little variation in his convective normalized heating rates with gas composition from 100% CO_2 to 85% CO_2 – 15% N_2. Again the present data obtained with the 5-in.-diam model are generally greater than the small model data as expected for increased radiative flux. The estimate of Van Tassell is used in the data analysis.

From available experimental data[21–23] and flowfield analysis,[24,25] an approximate expression relating the ratio of flat-faced cylinder radius to that of a sphere with equal stagnation point velocity gradient was found to be $r^*/R = (4/3\pi)[(\rho_2/\rho_3)(2 - \rho_2/\rho_3)]^{1/2}$. By use of this expression, the con-

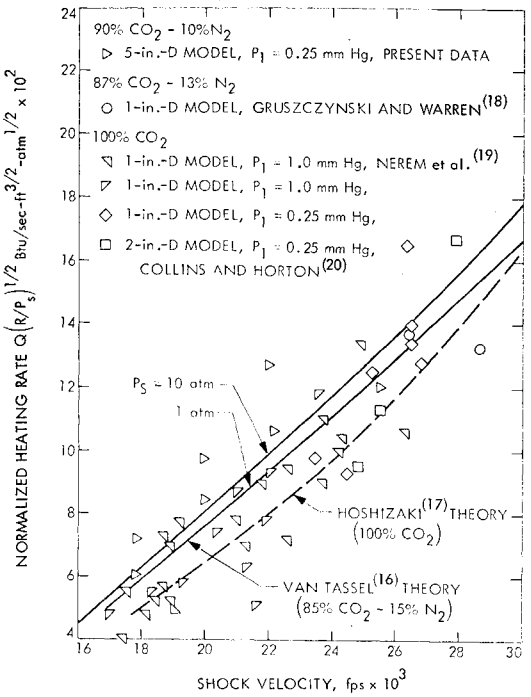

Fig. 9 Stagnation-point heating rates of shock-tube models in Venus gas.

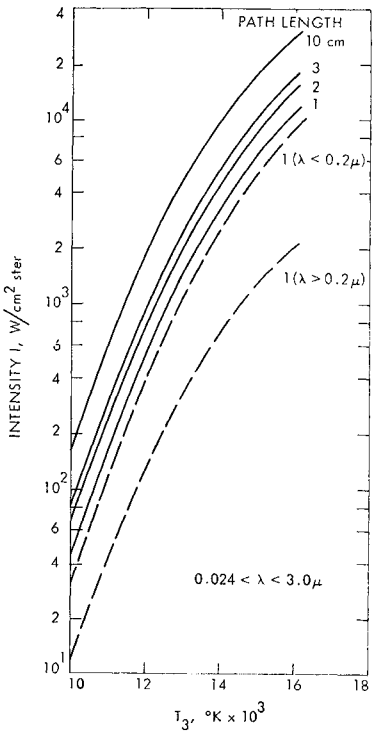

Fig. 10 Isothermal intensity behind model bow shock wave in air; P_1 = 0.25 torr.

vective heating rates to a truncated cylinder may be computed.

Estimated Isothermal Radiative Flux

Radiative intensity calculations have been performed by Stickford[26] of this laboratory for the major atomic processes in plasmas containing mixtures of carbon, nitrogen, and oxygen. The actual detail was computed from 240 to 30,000 Å for the continuum processes (i.e., free-free and free-bound recombination reactions) using atomic free-bound cross sections calculated by Thomas[27] of Jet Propulsion Laboratory in the extreme ultraviolet, and the quantum-defect cross sections of Anderson and Griem[28] in the visible. The atomic line data of Wilson and Nicolet[29] were used to compute the spectral line contribution in the ultraviolet region assuming the lines to have a dispersion profile. The radiative contribution of each continuum process as well as the contribution of each line was summed at every ½ Å from 600 to 1700 Å. In this manner, reabsorption due to line-line overlapping as well as continuum-line overlapping is accounted for. This treatment results in a very precise and, hopefully, accurate calculation of the ultraviolet radiation.

The visible lines were integrated individually assuming a dispersion shape and constant Planck function. Reabsorption due to continuum-line overlapping was accounted for; however, line-line overlapping was neglected. The error due to neglecting line-line overlapping in the visible is estimated to be less than 5% at moderare densities and path lengths.

The isothermal intensity for these test conditions is shown in Fig. 10 for air and in Fig. 11 for 90% CO_2–10% N_2. Calculations are shown for path lengths of 1, 2, 3, and 10 cm, with an indication of gross spectral distribution for a path length of 1 cm. Most of the energy is transported at ultraviolet wavelengths.

The CO(4+) band radiative intensity shown in Fig. 11 is taken from Ref. 30, where an electronic f-number of 0.148 was assumed for these far-ultraviolet bands, though recent radiative lifetime measurements of Hesser[31] indicate an f-number of 0.094. Other known molecular sources of radiation including CN(violet) are weak at these test conditions and hence are not included.

If the shock layer is assumed to be a plane slab of thickness equal to the Serbin shock standoff distance δ, the flux F has been computed for each model from the intensity I using the approximation $F_\delta = \pi I_{2\delta}$.[32] These calculated results are shown in Figs. 12 and 13 for air and Venus atmospheric gas, respectively. The flux has about a square root dependence on path length for both gases, thus indicating the optically thick behavior at these test conditions. When the isothermal radiative flux is corrected for the nonisothermal behavior

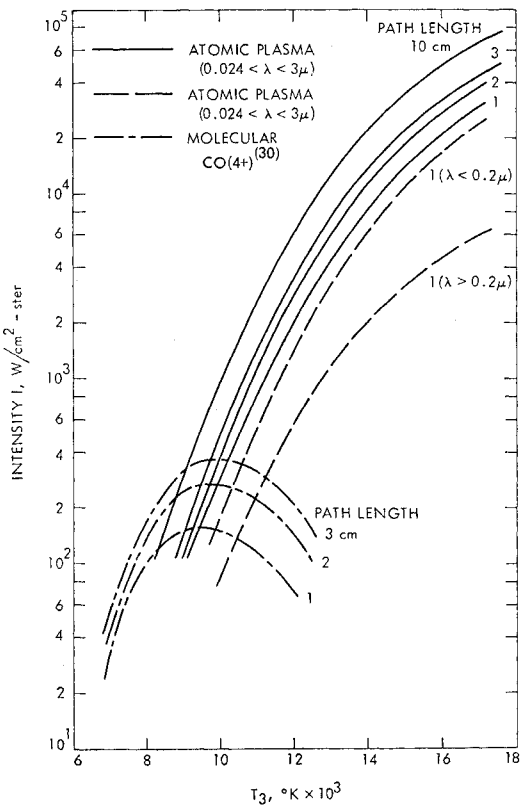

Fig. 11 Isothermal intensity behind model bow shock wave in Venus gas; P_1 = 0.25 torr.

resulting from radiative cooling as found by Page et al.[33] for an optically thick gas, the result is a flux estimate less than one-half the isothermal value at temperatures approaching 15,000°K. This nonisothermal thick gas correction factor was computed by Page for a shock standoff distance of 10 cm and pressure of 1 atm rather than the 0.7 to 1.4 cm standoff distances and pressure of about 4 atm of these tests; however, the optical path lengths δP do not differ greatly. The correction factor can be expressed as follows $F/F_{\text{isothermal}} = 0.200 - 0.295 \ln_{10} \Gamma$, for $0.04 < \Gamma < 1.0$, where $\Gamma = 2F_{\text{isothermal}}/\rho_3 u_3 H_s$.

IV. Heat-Transfer Results

Air Results

The calorimeter heat-transfer oscillographs provide a continuous record of the calorimeter temperature during the test run. The slope of these traces was evaluated at conditions corresponding to near-steady-state flow over the models as judged from the shock formation results. Except for the lowest shock velocity data, all of the good heat-transfer data obtained in air at an initial pressure of 0.25 mm Hg were almost independent of model size and shape as seen in Fig. 14. The magnitude of the heating rate measurements increased from about 1,500 Btu/sec-ft² at a shock speed of 18,500 fps to nearly 17,000 Btu/sec-ft² at 30,000 fps. Among the many shock-tube runs, five data points shown results with a carbon-coated platinum calorimeter, but indicate no particular difference from the uncoated gage data; therefore we conclude that most of the radiative flux is at ultraviolet wavelengths. Because of the difficulty in obtaining sufficiently long shock-tube run time at shock speeds near 30,000 fps, only one good run was obtained with the 2-in.-diam model.

Obtaining data with the $1\frac{1}{4}$-in.-diam truncated-cylinder model and the 5-in.-diam hemispherical model was possible at all shock speeds; however, since most models are destroyed as shock speeds above 25,000 fps, the simpler-to-build truncated-cylinder models are used more frequently. Also shown in Fig. 14 is the estimate of uncoupled convective heat transfer rate as calculated from the theory of DeRienzo and Pallone. The measured heat transfer rates were always greater than the theory for convective heat transfer alone.

The present calculated radiative flux reduced for coupling effects and summed with the computed uncoupled convective heating rates closely approximates the measured heat flux at shock speeds of from 23,000 to 30,000 fps. The summed theoretical heating rates do not differ for the several models since the reduction in convective heat transfer computed for larger models is offset by the increased radiative flux on these larger models. Even with the limited amount of data with the larger models, the data do verify the independence of total heat transfer rate with model size. The two successful runs made with the hemispherical models at these high temperature conditions confirmed our trust in the validity of the more numerous truncated-cylinder tests. A more complex and complete solution of the coupled flowfield and radiation field at these test conditions would be desirable for a better understanding and description of the flow.

Wood, Hoshizaki, Andrews, and Wilson[34] have shown reflected shock total radiative intensity data at air temperatures from 10,000 to 15,000°K which agree with Wilson and Grief[32] except at temperatures above 13,000°K where possible radiative cooling reduces the measured intensity as expected. Wood et al. also present a comparison of the Wilson and Grief theory with most of the available shock tube radiative intensity measurements. The present radiative flux calculations are close to that of Wilson and Grief at temperatures from 10,000 to 15,000°K.

Venus Atmosphere Results

A composite plot of all total heating data obtained in the 90% CO_2–10% N_2 gas mixture at an initial shock tube pressure of 0.25 mm Hg is shown in Fig. 15. Heating rates vary from 1,500 Btu/sec-ft² at shock speeds near 17,500 fps to heating rates of over 20,000 Btu/sec-ft² at shock speeds near 29,000 fps.

Again, as was the case with the air tests, a sufficient time of steady-state flow exists over all models at the lower shock speeds. At shock speeds greater than 27,000 fps it was impossible to obtain sufficient test time to establish flow over

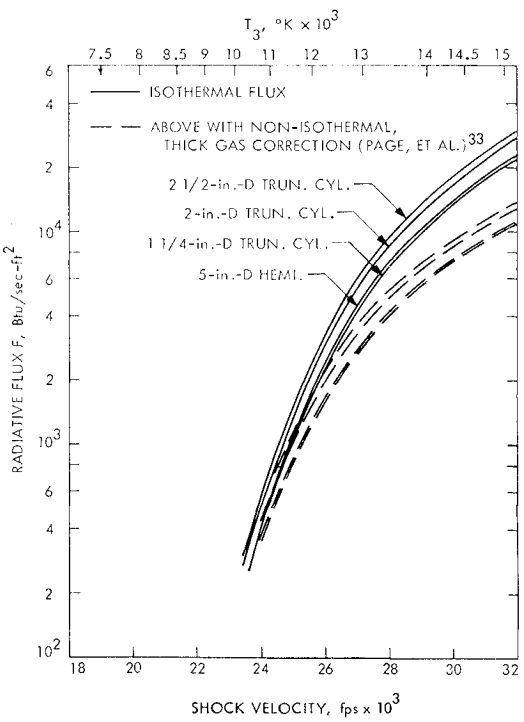

Fig. 12 Radiative flux to the stagnation-point of shock-tube models in air; $P_1 = 0.25$ torr.

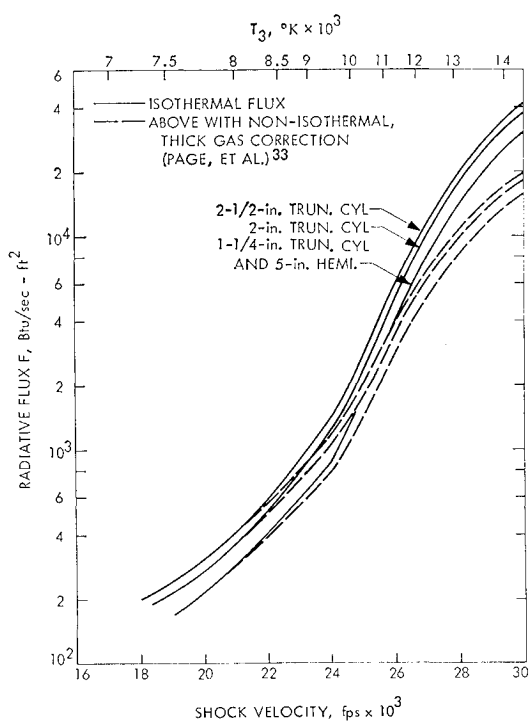

Fig. 13 Radiative flux to the stagnation-point of shock-tube models in Venus gas; $P_1 = 0.25$ torr.

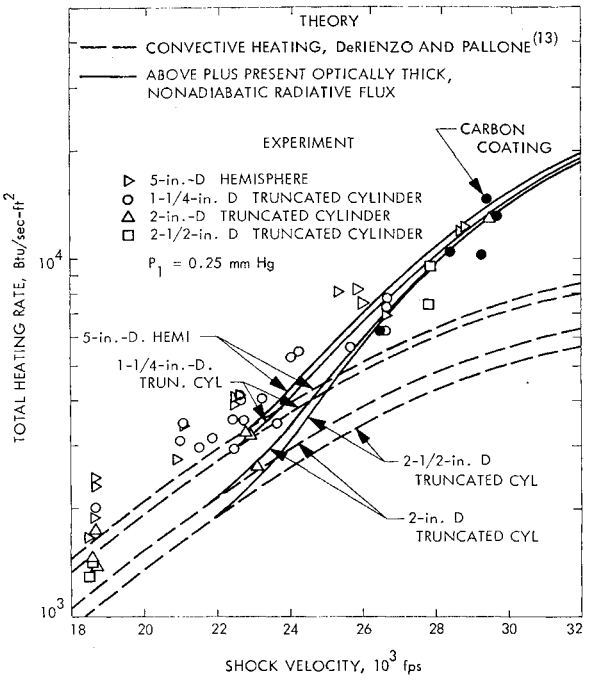

Fig. 14 Comparison of air results with theory.

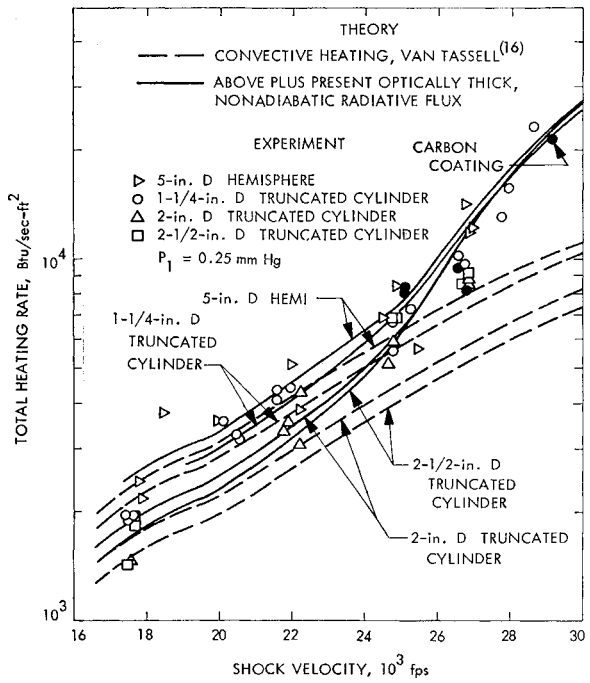

Fig. 15 Comparison of Venus gas results with theory.

the larger truncated-cylinder models. The stagnation point heating rate measurements were greater than at comparable shock velocities in air, however, most of this increase is due to the greater initial density of the 90% CO_2–10% N_2 mixture at a pressure of 0.25 mm Hg. At shock speeds between 17,500 and 22,000 fps, the heating rate to the larger truncated-cylinder models in the Venus mixture indicate lower rates than the smaller models as expected for a condition where convective heating dominates.

The convective heat transfer estimation of Van Tassell for a 85% CO_2–15% N_2 atmosphere is shown in the figure. Again the measured data are consistently higher than this estimate apparently due to molecular and atomic radiative flux. The heat transfer rates at the lower shock speeds are somewhat more than expected from the CO(4+) bands plus the estimated convective flux. Because of the previously cited uncertainty in the convective heat transfer of carbon dioxide-nitrogen mixtures, we are unable to verify any prediction of the radiative flux in the 17,500 to 22,000 fps shock speed range.

At shock speeds faster than 25,000 fps where the CO concentration is small, the radiative flux is dominated by atomic radiation. The calculated nonisothermal flux from atomic sources has been summed with the uncoupled estimate of convective heat transfer and is plotted in Fig. 15 with the data. Again as with the air theory, the radiative flux has been reduced by a factor allowing for radiative cooling of the shock-layer gases. A reduction expected for an optically thick gas as used in the air results brings the calculation into good agreement with the measured results. In this gas mixture, there seems to be no noticeable difference in the level of heat transfer rate with gage surface. Sufficient data have not been obtained with the larger models at the faster shock speeds to analyze the geometric effects; however, there seems little doubt that the theories would adequately describe future data at these test conditions.

V. Conclusion

The total heating rates at the stagnation point of hemispherical and flat-faced cylinder models in shock-heated air and Venus atmospheric plasma at shock speeds between 23,000 and 30,000 fps were close to that estimated by summing uncoupled convective heating theory with isothermal radiative flux calculations reduced by a radiative cooling factor. The coupling between the radiation field and the flowfield is significant at these conditions. Because of uncertainty in the convective heat transfer of 90% CO_2 – 10% N_2, we are unable to verify any prediction of radiative flux in the 17,500 to 22,000 fps shock speed range where CO(4+) radiation predominates.

The bow shock wave reflected from the hemispherical model approached its equilibrium position in a decaying exponential manner. Contrasted to this, the bow wave reflected from the truncated-cylinder models moved at near constant velocity until it abruptly halted at a near equilibrium position. The equilibrium shock standoff distance measured for all models agrees with the theory of Serbin.

References

[1] Goulard, R. et al., "Radiating Flows During Entry into Planetary Atmospheres," 19th Congress of the International Astronautical Federation, Paper RE 70, Oct. 13–19, 1968.

[2] Anderson, John D., Jr., "An Engineering Survey of Radiating Shock Layers," *AIAA Journal*, Vol. 7, No. 9, Sept. 1969, pp. 1665–1675.

[3] Williard, J. W., "Design and Performance of the JPL Free-Piston Shock Tube," *Fifth Hypervelocity Techniques Symposium*, Vol. 1, University of Denver, March 1967, pp. 157–205.

[4] Collins, D. J. et al., "Hypervelocity Shock Tube," TR 32-620, June 1964, Jet Propulsion Laboratory, Pasadena, Calif.

[5] Rose, P. H., "Development of the Calorimeter Heat Transfer Gauge for Use in Shock Tubes," *Review Scientific Instruments*, Vol. 29, July 1958, pp. 557–564.

[6] Horton, T. E. and Babineaux, T. L., "Influence of Atmospheric Composition on Hypersonic Stagnation-Point Convective Heating," *AIAA Journal*, Vol. 5, No. 1, Jan. 1967, pp. 36–43.

[7] Thomas, G. M. and Menard, W. A., "Experimental Measurements of Nonequilibrium and Equilibrium Radiation from Planetary Atmosphere," *AIAA Journal*, Vol. 4, No. 2, Feb. 1966, pp. 227–237.

[8] Horton, T. E. and Menard, W. A., "A Program for Computing Shock Tube Gasdynamic Properties," TR 32-1350, Dec. 1968, Jet Propulsion Laboratory, Pasadena, Calif.

[9] Menard, W. A. and Horton, T. E., "Shock-Tube Thermochemistry Tables for High-Temperature Gases-Air," TR 32-1408, Vol. 1, Nov. 1, 1969, Jet Propulsion Laboratory, Pasadena, Calif.

[10] Menard, W. A. and Horton, T. E., "Shock-Tube Thermochemistry Tables for High-Temperature Gases—90% Carbon Dioxide and 10% Nitrogen," TR 32-1408, Vol. 2, Dec. 1, 1969, Jet Propulsion Laboratory, Pasadena, Calif.

[11] Serbin, H., "Supersonic Flow Around Blunt Bodies," *Journal Aeronautical Sciences*, Vol. 25, No. 1, Jan. 1958, pp. 58–59.

[12] Rose, P. H. and Stankevics, J. O., "Stagnation-Point Heat Transfer Measurements in Partially Ionized Air," *AIAA Journal*, Vol. 1, No. 12, Dec. 1963, pp. 2752–2763.

[13] DeRienzo, P. and Pallone, A. J., "Convective Stagnation Point Heating for Re-Entry Speeds up to 70,000 fps Including Effects of Large Blowing Rates," *AIAA Journal*, Vol. 5, No. 2, Jan. 1967, pp. 193–200.

[14] Fay, J. A. and Kemp, N. G., "Theory of Stagnation-Point Heat Transfer in a Partially Ionized Diatomic Gas," *AIAA Journal*, Vol. 1, No. 12, Dec. 1963, pp. 2741–2751.

[15] Horton, T. E. and Zeh, D. W., "Effects of Uncertainties in Transport Properties on Prediction of Stagnation-Point Heat Transfer," *AIAA Journal*, Vol. 5, No. 8, Aug. 1967, pp. 1497–98.

[16] Van Tassell, W., "Convective Heating in Planetary Atmospheres," AVCO/RAD-TM-63-72, Oct. 1963, AVCO Corporation, Wilmington, Mass.

[17] Hoshizaki, H., "Heat Transfer in Planetary Atmospheres at Super-Satellite Speeds," *ARS Journal*, Vol. 32, No. 10, Oct. 1962, pp. 1544–1552.

[18] Gruszczynski, J. S. and Warren, W. R., Jr., "Experimental Heat Transfer Studies of Hypervelocity Flight in Planetary Atmospheres," *AIAA Journal*, Vol. 2, No. 9, Sept. 1964, pp. 1542–1550.

[19] Nerem, R. M., Morgan, J. C., and Graber, B. C., "Hypervelocity Stagnation Point Heat Transfer in a Carbon Dioxide Atmosphere," *AIAA Journal*, Vol. 1, No. 9, Sept. 1963, pp. 2173–2175.

[20] Collins, D. J. and Horton, T. E., "Experimental Convective Heat Transfer Measurements," *AIAA Journal*, Vol. 2, No. 11, Nov. 1964, pp. 2046–2047.

[21] Boison, J. C. and Curtiss, H. A., "An Experimental Investigation of Blunt Body Stagnation Point Velocity Gradient," *ARS Journal*, Vol. 29, No. 1, Jan. 1959, pp. 130–135.

[22] Ellison, J. C., "Experimental Stagnation-Point Velocity Gradients and Heat-Transfer Coefficients for a Family of Blunt Bodies at Mach 8 and Angles of Attack," Rept L-6141 (Review Copy), 1969, NASA.

[23] Stoney, W. E. and Markley, J. T., "Heat-Transfer and Pressure Measurement on Flat-Faced Cylinders at a Mach Number of 2," TN 4300, July 1958, NASA.

[24] Vinokur, M., "Hypersonic Flow Around Bodies of Revolution which are Generated by Conic Section," *6th Midwestern Conference on Fluid Mechanics*, University of Texas, Austin, Texas, Sept. 9–11, 1959.

[25] Inouye, M., Marvin, J. G., and Sinclair, A. R., "Comparison of Experimental and Theoretical Shock Shapes and Pressure Distributions on Flat-Faced Cylinders at Mach 10.5," TN D-4397, 1968, NASA.

[26] Stickford, G. H., "Total Radiative Intensity Calculations for 100% CO_2 and 90% CO_2–10% N_2," *Journal of Quantitative Spectroscopy and Radiative Transfer*, Vol. 10, 1970, pp. 249–270.

[27] Thomas, G. M. and Helliwell, T. M., "Photoionization Cross Sections of Nitrogen, Oxygen, Carbon and Argon for the Slater-Klein-Brueckner Potential," *Journal of Quantitative Spectroscopy and Radiative Transfer*, Vol. 10, 1970, pp. 423–448.

[28] Anderson, A. D. and Griem, H. R., "Continuum Emission Coefficients from the Quantum Defect Method," *Proceedings of the Sixth International Conference on Ionization Phenomena in Gases*, Vol. 3, North Holland Publishing Co., Amsterdam, 1963, pp. 293–98.

[29] Wilson, K. H. and Nicolet, W. E., "Spectral Absorption Coefficients of Carbon, Nitrogen and Oxygen Atoms," *Journal of Quantitative Spectroscopy and Radiative Transfer*, Vol. 7, 1967, pp. 891–941.

[30] Gruszczynski, J. S., "Hypervelocity Heat Transfer Studies in Simulated Planetary Atmospheres," Final Rept, JPL P. O. 950297, June 1967, General Electric Co, King of Prussia, Pa., pp. 88–92.

[31] Hesser, J. E., "Absolute Transition Probabilities in Ultraviolet Molecular Spectra," *Journal of Chemical Physics*, Vol. 48, 1968, pp. 2518–2535.

[32] Wilson, K. H. and Grief, R., "Radiation Transport in Atomic Plasmas," *Journal of Quantitative Spectroscopy and Radiative Transfer*, Vol. 8, April 1968, pp. 1061–1086.

[33] Page, W. A. et al., "Radiative Transport in Inviscid Nonadiabatic Stagnation-Region Shock Layers," *AIAA Progress in Astronautics and Aeronautics: Thermal Design Properties of Spacecraft and Entry Bodies*, Vol. 21, edited by J. T. Bevans, Academic Press, New York, 1969, pp. 75–114.

[34] Wood, A. D. et al., "Measurements of the Total Radiant Intensity of Air," *AIAA Journal*, Vol. 7, No. 1, Jan. 1969, pp. 130–139.